

Article

Broadband Vortex Beam Modulating System Based on Electrically Controlled Liquid Crystal Devices

Xinyi Zhou ¹, Zongjie Zhu ¹, Xiangsheng Xie ¹, Lishuang Yao ¹ , Fan Fan ² and Yaqin Zhou ^{1,*} 

¹ College of Science, Shantou University, Shantou 515063, China; 22xyzhou1@stu.edu.cn (X.Z.); 20zjzhu@stu.edu.cn (Z.Z.); xxs@stu.edu.cn (X.X.); lsyao@stu.edu.cn (L.Y.)

² Key Laboratory for Micro-/Nano-Optoelectronic Devices of Ministry of Education, School of Physics and Electronics, Hunan University, Changsha 410082, China; ffan@hnu.edu.cn

* Correspondence: yqzhou@stu.edu.cn

Abstract: Vortex beams with helical phase wavefronts have recently emerged as a research hotspot because of their widespread applications such as ultra-high dimensional information encoding, quantum entanglement, and data transmission due to their unique properties. Research, as of yet, on the easy preparation of vector vortex beams is hindered by technical bottlenecks such as large mechanical modulation errors and limited bandwidths of meta-structured devices in spite of the massive experimental and theoretical breakthroughs in the generation of vortex beams that have been made. To make up for the deficiency in this area, we propose here a broadband vortex beam modulating system based on electrically controlled liquid crystal (LC) devices. An electrically controlled LC q-plate and an LC broadband polarization grating (PG) are integrated in the system as the crux devices. The system enables pure vortex-phase modulation within a wide spectral range in the visible spectrum and electrical control on the output beam intensity of the vortex and Gaussian components. Experiments at different voltages of 533 nm and 632.8 nm were conducted for validation. This system overcomes the complexity and stringent optical path requirements of traditional methods for generating vortex beams, offering an efficient, convenient, and rapidly tunable approach for generating vortex beams that is easily and highly integrable.

Keywords: liquid crystal device; vortex beam; q-plate; broadband polarization grating



Citation: Zhou, X.; Zhu, Z.; Xie, X.; Yao, L.; Fan, F.; Zhou, Y. Broadband Vortex Beam Modulating System Based on Electrically Controlled Liquid Crystal Devices. *Photonics* **2023**, *10*, 1012. <https://doi.org/10.3390/photonics10091012>

Received: 2 August 2023

Revised: 28 August 2023

Accepted: 1 September 2023

Published: 4 September 2023



Copyright: © 2023 by the authors. Licensee MDPI, Basel, Switzerland. This article is an open access article distributed under the terms and conditions of the Creative Commons Attribution (CC BY) license (<https://creativecommons.org/licenses/by/4.0/>).

1. Introduction

Over 30 years have passed since P. Coulet observed a unique optical phenomenon in a laser cavity and discovered similarities to superfluid vortices [1]. This phenomenon was later named the optical vortex. Since then, the generation and application of vortex beams have emerged as a research hotspot because vortex beams with orbital angular momentum (OAM) have more freedom in the interaction between light and matter, and are widely used in new system laser radars, laser processing, high-density optical storage, high-resolution imaging, and other fields [2–7]. In 1992, Allen firstly discovered that the optical vortex in vortex beams carried orbital angular momentum during the propagation of near-axis beams. Based on this discovery, extensive research has been conducted on vortex beams [8]. Following this revelation, researchers delved into the manipulation of optical properties and it was in 1993 when M. W. Beijerbergen introduced a phase difference into an incident Hermite–Gaussian beam by using a pair of cylindrical lenses, enabling the preparation of Laguerre–Gaussian modes [9]. The potential for practical applications came to fruition in 1995, when he successfully harnessed OAM optimized optical tweezers to induce particle rotation [10]. By 1997, Soskin furtherly explored the complex behavior of vortex beams' topological charges during propagation, deepening our understanding of their unique characteristics [11]. Notably, M. Reicherter's pivotal work in 1999 leveraged liquid crystal displays to generate vortex beams and used them to trap and manipulate polystyrene particles [12]. In the early 21st century, the implications

of vortex beams extended into the realm of quantum phenomena. In 2001, Zeilinger and his team unveiled quantum entanglement within OAM states, paving the way for intriguing prospects in incorporating optical vortices or twisted photons into quantum applications [13]. In the same year, Paterson et al. achieved controlled rotation of optically trapped microparticles within a spiral interference pattern, offering significant applications in optical and biomedical micromechanics [6]. By 2008, Barreiro et al. introduced an encoding technique utilizing OAM, conferring significant advantages to vortex beams for their application in the field of optical communication [14]. By 2011, Capasso and colleagues unveiled a comprehensive framework for reflection and refraction, revolutionizing the generation of optical vortices on nanoscale metasurfaces. Their work greatly improved the design of light beams [15]. Steering towards 2013, Willner's team achieved a milestone by demonstrating terabit-scale optical communication through OAM multiplexing in fibers. This breakthrough highlighted OAM's potential for enhancing data multiplexing in future fiber networks [16]. Fast-forwarding to 2018, Xie et al. designed a wideband on-chip OAM transmitter, elevating information capacity in optical communication and solidifying its application in the field [17].

In essence, vortex beams represent a distinct class of beams characterized by their helical wavefronts and non-uniform polarization [18]. Propagating with spiral phase along their axes, vortex beams feature phase singularities at their centers with zero intensity. Their remarkable property of possessing both angular and rotational momentum confers heightened channel capacity through the OAM generated by the helical phase wavefronts. The phase gradient force further expands their practicality across diverse fields, from high-density optical storage to precision optical manipulation. Precisely owing to these factors, the methodologies for generating vortex beams have ignited profound interest among researchers, giving rise to an extensive array of proposed techniques for vortex beam generation. Notable milestones include M. W. Beijersbergen's pioneering work in 1994, which demonstrated through experimentation that a spiral phase plate could convert TEM laser beams into spiral wavefront beams with phase singularities along the axis. This innovative work provided a novel approach to generating a vortex phase [19]. By 2002, Biener et al. proposed a method for creating a spiral phase front using artificial, anisotropic, non-uniform media based on subwavelength gratings [20]. Fast-forwarding to 2015, L.X. Chen et al. harnessed spatial light modulators to produce multiple superposition states of vortex beams [21]. In 2017, C. Alpmann et al. achieved a breakthrough in generating intricate Poincaré beams through innovative techniques such as amplitude and phase modulation, coupled with spatial polarization structuring, opening new avenues for quantum communication and optical manipulation [22]. By 2020, the research group of Y. Ren achieved the preparation of high-order vortex beams by proposing a cross-phase method in which no optical components were involved [23]. The year 2021 marked a significant leap, with M. Liu et al. demonstrating the feasibility of utilizing all-dielectric metasurfaces to generate generalized perfect Poincaré beams, showcasing potential applications in optical information encryption [24]. Despite the considerable research efforts dedicated to vortex beam generation, certain limitations such as large mechanical modulation errors and limited bandwidths of meta-structured devices still persist in existing methods [25–31].

The utilization of phase, amplitude, and polarization are the most important method to control and manipulate light field. As an innovative form of phase plate, Pancharatnam-Berry (PB) phase optics exhibits remarkable performance in both phase control and polarization manipulation. They are inherently polarization sensitive, in contrast to dynamic phase devices. At present, an increasing number of PB phase optical components have been developed, including polarization gratings (PGs), q-plates, forked polarization gratings (FPGs), and Airy beam cubic phase plates, among others. In order to generate vortex beams precisely and without narrow bandwidth limitation, we propose a novel broadband vortex beam modulating system based on electrically controlled LC devices that mainly consist of an LC q-plate and an LC broadband PG. Theoretically, the system holds the potential to achieve phase modulation for wide-spectrum vortex beams. Experimental investigation has

been conducted on the diffracted optical patterns within the +1st diffraction order’s vortex component, employing lasers with wavelengths of 533 nm and 632.8 nm. The experimental results substantiate the practical viability of the proposed theoretical model. This system enables broadband pure phase control. Furthermore, by incorporating electrically controlled LC devices, independent intensity modulation can be achieved. As a versatile broadband vortex beam generator, this system not only facilitates the generation and modulation of a perfect vortex phase but also allows precise control of the output intensity of the vortex part and Gaussian part by adjusting the voltage applied on the electrically controlled LC q-plate [32–34]. Our work provides a fully electrically controlled,, convenient, efficient, low-cost, high-precision, and easily integrative optical system for vortex beam generating and modulating, and is expected to expand the applications of vortex beams in national defense and military fields such as optical communication, laser processing, high-density optical storage, high-resolution imaging, and quantum technology [35–41].

2. Theoretic Basis

We use two visible lasers with different wavelengths ($\lambda_1 = 632.8$ nm and $\lambda_2 = 533$ nm) as the incident laser source to verify the broadband profile of this vortex beam modulating system. Firstly, the incident beams are converted into left-handed circularly (LHC) polarized beam through a Gran polarizer and a quarter-wave plate (QWP). We can express the incident beams in terms of the Jones vector as follows:

$$\psi_{in_1} \text{ or } \psi_{in_2} = \begin{bmatrix} 1 \\ j \end{bmatrix}. \tag{1}$$

The Jones matrix of q-plate with electrically controlled phase retardation is as follows [42]:

$$M_{q\text{-plate}} = \cos \frac{\Gamma}{2} \begin{bmatrix} 1 & 0 \\ 0 & 1 \end{bmatrix} - j \sin \frac{\Gamma}{2} \begin{bmatrix} \cos 2\varphi & \sin 2\varphi \\ \sin 2\varphi & -\cos 2\varphi \end{bmatrix}, \tag{2}$$

wherein the orientation of the optical axis $\varphi = q\theta + \varphi_0$ and phase retardation $\Gamma = 2\pi d\Delta n / \lambda$. θ represents the azimuthal angel in Cartesian coordinate system, q represents the topological charge of the q-plate, and φ_0 is the initial angle between the orientation of the optical axis and the x -axis when $\theta = 0$. In this work, we use a q-plate with $\varphi = \theta$.

When two incident beams of different wavelengths enter the q-plate, their retardation can be controlled by voltage, the output beam is as follows:

$$\psi_{out} = M_{q\text{-plate}}\psi_{in}. \tag{3}$$

While $\Gamma_1 = 2\pi d\Delta n / \lambda_1$ for ψ_{in_1} and $\Gamma_2 = 2\pi d\Delta n / \lambda_2$ for ψ_{in_2} and Δn is related to the voltage applied on the q-plate. Then, the Jones vector of the output beams can be written as follows:

$$\psi_{out_1} = \cos \frac{\Gamma_1}{2} \begin{bmatrix} 1 \\ j \end{bmatrix} - j \sin \frac{\Gamma_1}{2} \exp(j2\theta) \begin{bmatrix} 1 \\ -j \end{bmatrix}, \tag{4}$$

$$\psi_{out_2} = \cos \frac{\Gamma_2}{2} \begin{bmatrix} 1 \\ j \end{bmatrix} - j \sin \frac{\Gamma_2}{2} \exp(j2\theta) \begin{bmatrix} 1 \\ -j \end{bmatrix}. \tag{5}$$

The Jones matrix of a broadband PG with retardation $\Gamma = \pi$. The slow axis rotates along x -axis with an angle $\phi = \pi x / p$ and the p denotes the period of the grating [43]:

$$M_{PG} = -j \begin{bmatrix} \cos \frac{2\pi x}{p} & \sin \frac{2\pi x}{p} \\ \sin \frac{2\pi x}{p} & -\cos \frac{2\pi x}{p} \end{bmatrix}. \tag{6}$$

When two beams (ψ_{out1} and ψ_{out2}) pass through the broadband PG, the final output beams can be written as follows:

$$\psi_1 = -j \cos \frac{\Gamma_1}{2} \exp(j \frac{2\pi x}{p}) \begin{bmatrix} 1 \\ -j \end{bmatrix} - \sin \frac{\Gamma_1}{2} \exp[j(2\theta - \frac{2\pi x}{p})] \begin{bmatrix} 1 \\ j \end{bmatrix}, \quad (7)$$

$$\psi_2 = -j \cos \frac{\Gamma_2}{2} \exp(j \frac{2\pi x}{p}) \begin{bmatrix} 1 \\ -j \end{bmatrix} - \sin \frac{\Gamma_2}{2} \exp[j(2\theta - \frac{2\pi x}{p})] \begin{bmatrix} 1 \\ j \end{bmatrix}. \quad (8)$$

The corresponding wavelengths of the two beams are $\lambda_1 = 632.8$ nm and $\lambda_2 = 533$ nm. The output beams consist of a Gaussian beam and a vortex beam, whose intensity are controlled by the applied voltage on the q-plate. The phase $\exp(2\pi jx/p)$ in Equations (7) and (8) contributes to the spatial separation of LHC and RHC polarized beams. Owing to the following:

$$\sin \theta = \lambda/p \quad (9)$$

wherein θ is the separation angle between the LHC and RHC polarized beams, the angle varies with different wavelengths. Thus, the positions of the vortex part and Gaussian part of the output beams with distinct wavelengths are different.

3. Experiments and Results

To validate the broadband vortex beam modulating system based on electrically controlled LC devices, in this work we fabricated an electrically controlled LC q-plate through LC photo-alignment technology. The photoalignment technique offers a number of significant advantages over the “rubbing” treatment of LC cells as it is a highly accurate and non-contact method that avoids rubbing-induced dust impurities and damage to substrates. This method can effectively control the parameters of LC such as anchoring energy, pretilt angle, and orientation, making it particularly suitable and productive for the fabrication of such an LC q-plate. Firstly, 0.5 wt% azo dye SD1 was dissolved into dimethylformamide (DMF) as an oriented layer and spin-coated on two ITO substrates. After that 4 μ m spacers were sprayed on one of the substrates, followed by rapid glue encapsulation as a cell. The assembly was then placed on a digital micromirror device (DMD) platform for photo-alignment, where a pre-designed alignment layer with phase variation was imported into the DMD [44]. Finally, the E7 (from Jiangsu Hecheng Advanced Materials Co., Ltd., Huaihua, China) was injected into the cell to obtain an electrically controlled LC cell with a specific orientation angle. The structure of electrically controlled LC q-plate is shown in Figure 1a. By changing the applied voltage of the LC cell, rapid control of both the intensity and the transmitted wavelength of the light can be achieved.

We fabricated the broadband PG through the interference exposure method, as illustrated in Figure 1b. In this process, a 0.5 wt% solution of azo dye SD1 was dissolved in DMF. The solution was then coated onto a glass substrate and spun at 800 rpm for 5 s, followed by spinning at 2000 rpm for 30 s to obtain a uniform film as the alignment layer (Sample). A laser emitting 450 nm linearly polarized light passed through a half-wave plate, adjusting the polarization direction to 45°. The light then underwent spatial filtering using a filtering system comprised of a Gaussian cut-of (GCO) and an adjustable iris (IRIS) to remove higher-order modes and noise, resulting in a clean Gaussian beam. After collimation by a lens, the beam was split into two orthogonal linearly polarized light (transmitted p-light and reflected s-light) by a polarized beam splitter (PBS). The transmitted light was adjusted to overlap with the reflected light using a mirror (MR), and a QWP whose fast-axis orientation is 45° was placed in front of the overlapping region to convert the beams into LHC polarized beam and RHC polarized beams, respectively (with an included angle of 10.36°). The interference patterns were recorded on the alignment layer of the substrate exposed to the beams. Subsequently, a 25% RM-P01 solution (a polymerizable LC material) was mixed with chiral dopants (S811 with left-handed helicity and R811 with right-handed helicity, both at a concentration of 0.784%). We then sequentially spin-coated the LC solution doped

with different chiral dopants onto the sample. After exposure to nitrogen environment and curing light (365 nm) for 1 min, a broadband PG with a period of 2.5 μm was successfully fabricated. We apply this polarization interferometry for exposing PG because of the large optical path difference between the two beams. The time coherence of the laser is required, and the optical path difference must be ensured to be less than the laser coherence length $L = \lambda^2 / \Delta\lambda$, where λ^2 and $\Delta\lambda$ respectively represent the laser wavelength and spectral line width.

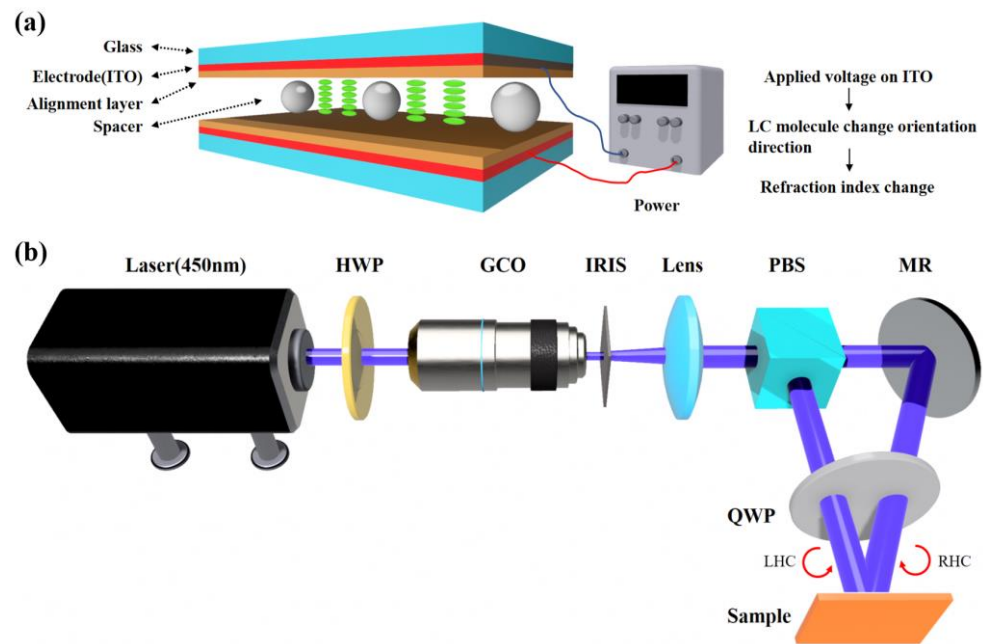


Figure 1. (a) Schematic diagram of the LC q-plate made using polarization holographic technology. (b) Schematic diagram for fabrication process of broadband PG by interference exposure method.

Unlike the conventional diffraction gratings that periodically operate the amplitude or dynamical phase of light, LC PGs periodically modulate the PB phases of light by spatially changing the anisotropy parameters across the plane of the elements in a periodic way. Broadband PGs has more than four-fold the bandwidth of traditional PGs (and is significantly larger than any other grating). The diffraction angle and operational region (visible, near-infrared, mid-wave infrared, and ultraviolet wavelengths) may be easily obtained during the manufacturing process. We demonstrate a broadband and thin-film polarization grating based on an anisotropic diffraction grating composed of reactive mesogens (polymerizable LCs). The broadband PG used in our experiment is depicted in Figure 2. This device leverages the achromatic properties of two antisymmetric chiral layers which act as self-compensators eliminating the dispersion in linear and warp-induced circular birefringence. When a linearly polarized light is incident on the broadband PG, the output beam can be decomposed into two circularly polarized beams with opposite handedness: LHC polarized beam with diffraction order $m = +1$ and RHC polarized beam with diffraction order $m = -1$, as shown in Figure 1a. The broadband PG consists of two chiral PG layers, as illustrated in Figure 1b. PG 2 has a slight relative phase shift with respect to the birefringent profile of PG 1. Both layers have the same thickness and opposite twist angle Φ [45].

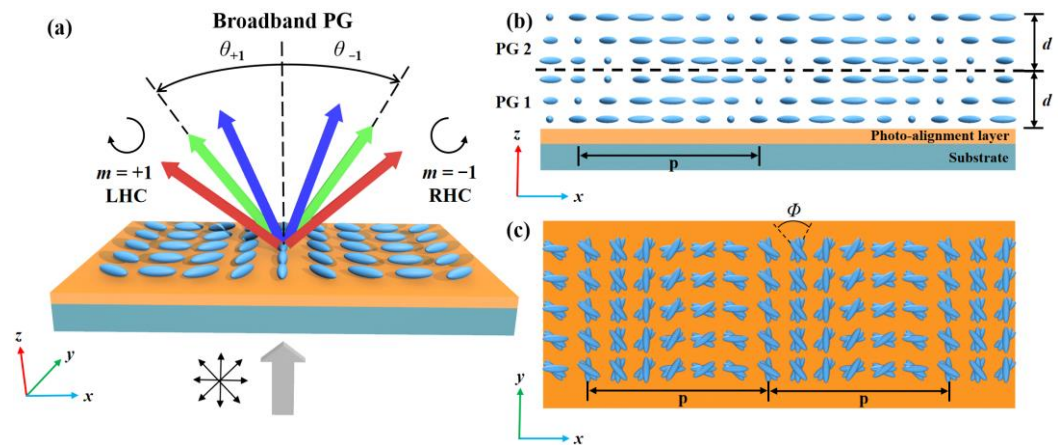


Figure 2. Schematic diagram of broadband PG. (a) Broadband PG structure and the diffraction property. (b) Front view and (c) side view of the PG.

Figure 3a shows the broadband PG observed under the polarization microscope. The period of the measured broadband PG is $2.5 \mu\text{m}$; Figure 3c shows the use of ordinary PG to observe the screw placed in the back. Due to its large zero-order diffraction leakage, the specific shape of the screw can be clearly observed. Figure 3d is the screw observed at the same distance using broadband PG.

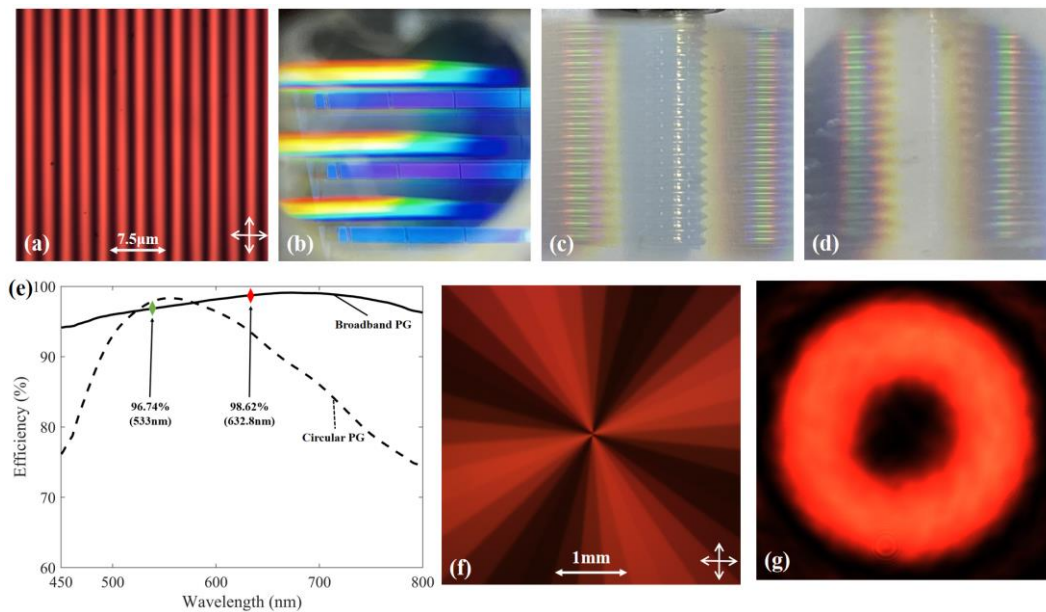


Figure 3. (a) Broadband PG observed under crossed-polarized microscope. (b) Optical image of white light passing through the broadband PG. (c,d) The screws observed by ordinary LC PG and broadband PG, respectively, at the same distance. (e) The 1st-order efficiency spectrum from spectrometer (curves) and laser (diamonds) measurements. (f) LC q-plate structure under $50\times$ polarization microscope. (g) Vortex beam generated by our LC q-plate.

This broadband PG exhibits practically ideal properties, with high 1st-order efficiency, high polarization selectivity, low scattering, and low non-first-order leakage. Therefore, zero-order leakage of broadband PG is significantly reduced by comparison with ordinary LC PG. Spectrometers are used to measure the 1st-order efficiency spectrum of ordinary LC PG and broadband PG. The transmittance of ordinary LC PG is larger only when the half-wave condition is satisfied. For broadband PG, the transmittance is greater than 95% in the band from 450 nm to 800 nm, and the transmittance is measured separately at

533 nm and 632.8 nm, which are 96.74% and 98.62%, respectively. The result is shown in Figure 3e. We measured the diffraction efficiency of broadband PG with wavelengths of 533 nm and 632.8 nm, and the uniform linear polarized light produced by a monochromatic laser was divided into three beams of ± 1 and 0 order through PG; here, the efficiency is calculated as $\eta = (I_{+1} + I_{-1}) / (I_{+1} + I_0 + I_{-1})$, where I_m is the light intensity of the diffraction order measured with optical power and energy meter (Thorlabs, PM100D). The calculated average diffraction efficiency of broadband PG is up to 97.63%. Figure 3f shows the LC q-plate image under polarization microscope, and there is a changing phase structure on the surface. Figure 3g is the intensity pattern of vortex beam with topological charge $m = 2$ generated by an LC q-plate.

Experimental setup for the broadband vortex beam modulating system is shown in Figure 4, two lasers with different wavelengths ($\lambda_1 = 632.8$ nm and $\lambda_2 = 533$ nm) are used as the laser sources. Firstly, we used Gran polarizer and QWP to convert the incident beams into LHC polarized beams. Then, the beams were coupled together by a BS. After that, the beam propagated into a series of devices consisting of a q-plate with voltage-controlled phase retardation and a broadband PG, and was finally observed by an observer. We changed the voltage applied on the LC q-plate to adjust the phase retardation of the device, which can modulate the light intensity and the vortex beams of different wavelengths. It should be noted that the incident beams need to coincide exactly when they are incident into a BS. This ensures that the different diffraction angles to different wavelengths generated by broadband PG to be the only reason for the spatial separation of the diffracted light spots. At the same time, the distance from broadband PG to the observer should be kept in the range of 40 cm to 60 cm.

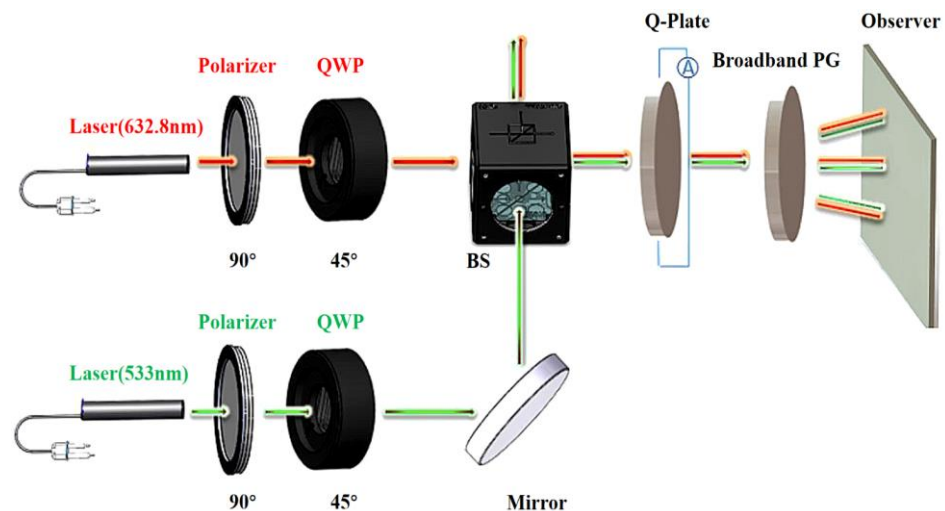


Figure 4. Experimental setup for the broadband vortex beam modulating system.

The corresponding diagram of the vortex beams and output beams under different voltages are shown in Figure 5a. To facilitate the observation of experimental results, we observed the vortex part by a CCD while the output beam was observed by a camera mounted at a fixed point. Intensity switching of vortex beams with different wavelengths was achieved by manipulating the phase retardation through variations of the voltage applied on the LC q-plate. When different voltages are loaded on the q-plate, the intensities of the Gaussian beam and vortex beam are different. We can see from Figure 5a that when the applied voltage is 1.7 V, $\Gamma_1 = 2\pi d\Delta n / \lambda_1 = 2\pi$, $\sin(\Gamma_1 / 2) = 0$, so the intensity of the vortex part reaches the minimum when the wavelength of the input beam is λ_1 . When the applied voltage is 2.0 V, $\Gamma_2 = 2\pi d\Delta n / \lambda_2 = 2\pi$, $\sin(\Gamma_2 / 2) = 0$, the intensity of the vortex part reaches the minimum when the wavelength of input beam is λ_2 . When the applied voltage is 2.7 V, $\Gamma_1 = 2\pi d\Delta n / \lambda_1 = \pi$, $\sin(\Gamma_1 / 2) = 1$, the intensity of the vortex part for λ_1 reaches the maximum. When the applied voltage is 3.0 V,

$\Gamma_2 = 2\pi d\Delta n / \lambda_2 = \pi$, $\sin(\Gamma_2 / 2) = 1$, the intensity of the vortex part for λ_2 reaches the maximum. When the applied voltage is up to 20.0 V, $\Gamma_1 \rightarrow 0$ and $\Gamma_2 \rightarrow 0$, the intensity of the vortex part for both input beam reaches the minimum.

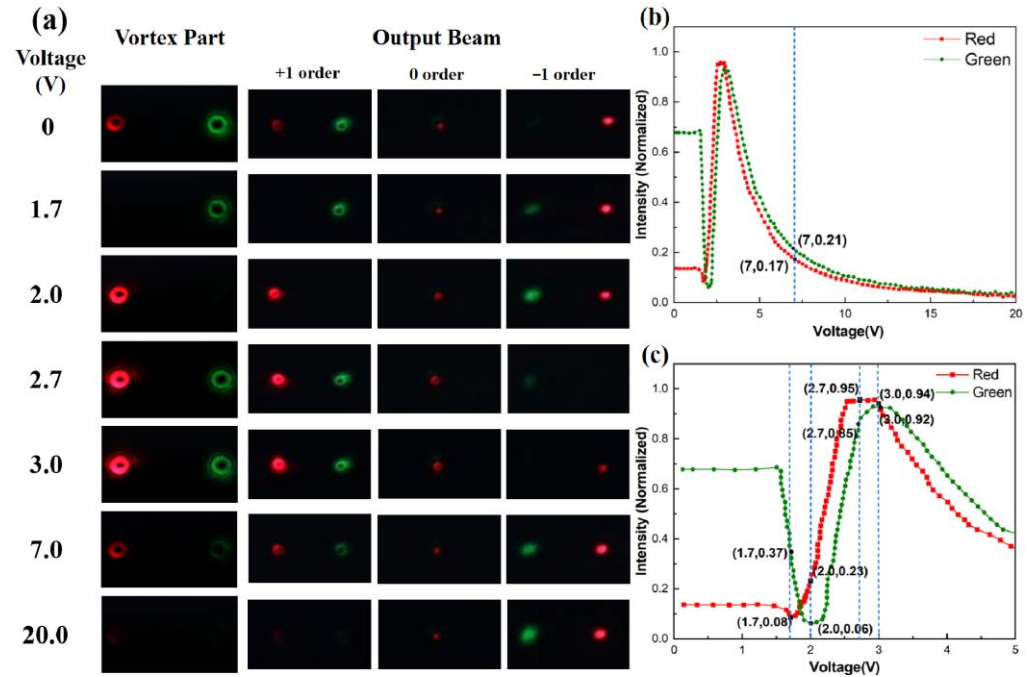


Figure 5. (a) Experimental results of vortex parts of the output beams and the whole output beams at different voltages; (b,c) intensity of the vortex parts of the output beams at different voltages. (c) Amplified representation of (b), illustrating the variation in light intensity within the voltage range of 0 to 5 V. The red line represents the intensity of the vortex parts of the output beams when the wavelength of the input light source is 632.8 nm; the green line shows the intensity variation tendency of the vortex parts of the output beams when the wavelength of the input light source is 533 nm.

Hence, we can obtain the intensity modulation of vortex beam and Gaussian beam electrically by altering the phase retardation of the incident beams. Additionally, PGs are optical structures formed by periodic variations in either transmittance or substrate refractive index. When light at wavelengths of 533 nm and 632.8 nm passes through PG, diffraction occurs. In accordance with the wave nature of light, its propagation can be described using wave vectors. The magnitude and direction of the wave vector are dependent on the frequency and propagation direction of the light. Described by the diffraction formula $\sin(\theta_m) = m\lambda / p$, the spatial separation phenomenon of light of varying wavelengths at ± 1 orders on a receiving screen can be elucidated: Here, θ_m signifies the diffraction angle, m denotes the diffraction order, and λ stands for the wavelength of the incident light. The θ_m governs the position of diffracted light on the receiving screen. Evident from the formula, the disparate wavelengths of light, due to distinct values of λ , lead to varying θ_m , subsequently yielding differing degrees of spatial separation on the observer’s plane.

The intensity of the vortex parts of the output beams under different voltages are separately measured with optical power and energy meter (Thorlabs, PM100D). In the absence of an electrically controlled q-plate within the optical path, the unaltered optical intensity denoted as I_s was recorded when laser light (at wavelengths of 533 nm and 632.8 nm) underwent diffraction through broadband PG. Subsequently, following the incorporation of an electrically controlled q-plate into the optical path, a progressive variation of voltage spanning the range from 0 V to 20 V across the terminals of the electrically controlled q-plate was executed, concomitant with the measurement of corresponding

optical intensities denoted as I_p . The normalized optical intensity, I_p / I_s , was determined. Notably, both measurements were conducted at an equidistant distance between the PG and the observer. The results are shown in Figure 5b,c. We can see from Figure 5c that as the voltage increases, the light intensity vortex beams with different wavelengths approach maximum and minimum at different voltages. When the voltage is 1.7 V, the vortex part of red light (632.8 nm) reaches minimum; the vortex part of green light (533 nm) reaches minimum when the voltage is 2.0 V. When the voltage is 2.7 V, the vortex part of red light (632.8 nm) reaches maximum; the vortex part of green light (533 nm) reaches maximum when the voltage is 3.0 V.

The transmittance of the broadband polarization grating produced by us is above 95% in the wavelength range from 450 nm to 800 nm. In this paper, the verification results of the vortex beams of 533 and 632.8 nm are satisfactory. The LC q-plate is affected by the external electric field, and the LC molecule will rotate gradually parallel to the direction of the electric field, thus forming an anisotropic LC layer. The LC molecules have a fixed out-of-plane angle (α , also called pretilt angle) and the birefringence of LC molecules is $n_e - n_o$. When the pretilt angle α gradually increases with the increase in voltage, the Δn of LC molecule in the z-axis direction gradually approaches n_o . The mathematical relationship between α and can be described as follows:

$$\Delta n = \frac{n_e n_o}{[n_o^2 + (n_e^2 - n_o^2) \sin^2 \alpha]^{\frac{1}{2}}} - n_o \quad (10)$$

Phase retardation $\Gamma = 2\pi d \Delta n / \lambda$, where d is the gap distance of the LC q-plate. The relation between Δn and external voltage can be deduced by elastic continuum theory of LCs; the LC polymer allows high polarization conversion efficient (PCE) and full-range phase modulation for single wavelength light. Therefore, when the voltage is 1.7 V and the red light (632.8 nm) meets the half-wave condition of $\Gamma_1 = \pi$, the intensity of the +1st diffraction spot received on the observer is approaching 0. Similarly, when the voltage is 2.0 V and the green light (533 nm) meets the half-wave condition of $\Gamma_2 = \pi$, the intensity of the +1st diffraction spot received on the observer is approaching 0. Thus, we realize the spatial modulation of vortex beams with different wavelengths by controlling voltage.

4. Discussion

We can achieve the modulation effect of the intensity of the vortex beam with different wavelengths. This setup improved the purity of the vortex beams when the half-wave condition of the q-plate is impossible to perfectly match, as the broadband PG can diverge the LHC and RHC polarized beams spatially. Additionally, the intensity of the output vortex part and Gaussian part can be controlled electrically, which is of great significance when intensity-alterable vortex beam is needed. More importantly, there are more application space of this system when LC q-plate is replaced by other PB phase optical elements.

On the other hand, there is still room for improvement in the analysis of the effect of the vortex beam generated by the system. Experimental defects originate mainly from the imperfect preparation of LC devices as well as the insufficient collimation of the light path. To enhance the LC device quality, experimental operations need to be conducted in a dust-free environment. Care should be taken to ensure proper collimation of the optical path during the orientation process while avoiding the introduction of mechanical vibrations. Additionally, it is advisable to select glass with superior light transmittance and maintain sufficient cleanliness during the glass cleaning process to prevent impurity contamination.

5. Conclusions

In conclusion, we have introduced a novel broadband vortex beams modulation system based on electrically controlled LC devices. This system offers the capability of achieving pure vortex phase modulation over a wide spectral range within the visible spectrum. We experimentally verified the generation and manipulation of vortex beams at 533 nm and 632.8 nm. Furthermore, the precise control of the output beam's vortex and

Gaussian components can be achieved by manipulating the voltage applied on the LC-q plate. The cost-effectiveness and high level of integration of LC devices present a more convenient and efficient method for generating vortex beams. The electronic control method in manipulation of structured light completely avoids the error caused by the manual operation, providing the possibility for the design of electrically controllable vector vortex beam lasers, and offering unprecedented application of vector vortex beams in quantum communication, laser processing, super-resolution imaging, as well as optical sensors.

Author Contributions: Conceptualization, Y.Z., F.F. and X.Z.; methodology, Y.Z. and X.Z.; validation, X.Z., Z.Z. and Y.Z.; formal analysis, X.Z.; investigation, X.Z.; resources, Y.Z.; data curation, X.Z.; writing—original draft preparation, X.Z., Z.Z. and Y.Z.; writing—review and editing, X.Z., Z.Z. and Y.Z.; visualization, X.Z.; supervision, Y.Z.; project administration, Y.Z.; funding acquisition, F.F., Y.Z., L.Y. and X.X. All authors have read and agreed to the published version of the manuscript.

Funding: This work was funded by the STU Scientific Research Initiation Grant (NTF21051); National Key Research and Development Program of China (2021YFB3600300); Guangdong Basic and Applied Basic Research Foundation (2021A1515012050); National Natural Science Foundation of China-Guangdong Joint Fund (2021A1515011931).

Institutional Review Board Statement: Not applicable.

Informed Consent Statement: Not applicable.

Data Availability Statement: Not applicable.

Conflicts of Interest: The authors declare no conflict of interest.

References

1. Couillet, P.; Gil, L.; Rocca, F. Optical vortices. *Opt. Commun.* **1989**, *73*, 403–408. [[CrossRef](#)]
2. Ding, D.S.; Zhang, W.; Zhou, Z.Y.; Shi, S.; Xiang, G.Y.; Wang, X.S.; Jiang, Y.K.; Shi, B.S.; Guo, G.C. Quantum Storage of Orbital Angular Momentum Entanglement in an Atomic Ensemble. *Phys. Rev. Lett.* **2015**, *114*, 5. [[CrossRef](#)] [[PubMed](#)]
3. Ding, Y.; Liu, T.; Liu, Z.L.; Qiu, S.; Xu, L.Y.; Ren, Y. Detection of a spinning object with circular procession using an optical vortex beam. *Opt. Lett.* **2022**, *47*, 2398–2401. [[CrossRef](#)] [[PubMed](#)]
4. Li, S.H.; Wang, J. Experimental demonstration of optical interconnects exploiting orbital angular momentum array. *Opt. Express* **2017**, *25*, 21537–21547. [[CrossRef](#)] [[PubMed](#)]
5. Toyoda, K.; Miyamoto, K.; Aoki, N.; Morita, R.; Omatsu, T. Using Optical Vortex to Control the Chirality of Twisted Metal Nanostructures. *Nano Lett.* **2012**, *12*, 3645–3649. [[CrossRef](#)]
6. Paterson, L. Controlled rotation of optically trapped microscopic particles. *Science* **2001**, *292*, 912–914. [[CrossRef](#)]
7. Zhang, Y.Z.; Zhao, H.; Wu, H.; Chen, Z.Y.; Pu, J.X. Recognition of Orbital Angular Momentum of Vortex Beams Based on Convolutional Neural Network and Multi-Objective Classifier. *Photonics* **2023**, *10*, 11. [[CrossRef](#)]
8. Allen, L.; Beijersbergen, M.W.; Spreeuw, R.J.C.; Woerdman, J.P. Orbital angular momentum of light and transformation of Laguerre Gaussian Laser modes. *Phys. Rev. A* **1992**, *45*, 8185–8189. [[CrossRef](#)]
9. Beijersbergen, M.W.; Allen, L.; Veen, H.E.L.O.v.d.; Woerdman, J.P. Astigmatic laser mode converters and transfer of orbital angular momentum. *Opt. Commun.* **1993**, *96*, 123–132. [[CrossRef](#)]
10. He, H.; Friese, M.E.J.; Heckenberg, N.R.; Rubinsztein-Dunlop, H. Direct Observation of Transfer of Angular Momentum to Absorptive Particles from a Laser Beam with a Phase Singularity. *Phys. Rev. Lett.* **1995**, *75*, 826–829. [[CrossRef](#)]
11. Soskin, M.S.; Gorshkov, V.N.; Vasnetsov, M.V.; Malos, J.T.; Heckenberg, N.R. Topological charge and angular momentum of light beams carrying optical vortices. *Phys. Rev. A* **1997**, *56*, 4064–4075.
12. Reicherter, M.R.; Haist, T.; Wagemann, E.U.; Tiziani, H.J. Optical particle trapping with computer-generated holograms written on a liquid-crystal display. *Opt. Lett.* **1999**, *24*, 608–610. [[PubMed](#)]
13. Mair, A.; Vaziri, A.; Weihs, G.; Zeilinger, A. Entanglement of the orbital angular momentum states of photons. *Nature* **2001**, *412*, 313–316. [[PubMed](#)]
14. Barreiro, J.T.; Wei, T.C.; Kwiat, P.G. Beating the channel capacity limit for linear photonic superdense coding. *Nat. Phys.* **2008**, *4*, 282–286.
15. Yu, N.F.; Genevet, P.; Kats, M.A.; Aieta, F.; Tetienne, J.P.; Capasso, F.; Gaburro, Z. Light Propagation with Phase Discontinuities: Generalized Laws of Reflection and Refraction. *Science* **2011**, *334*, 333–337.
16. Bozinovic, N.; Yue, Y.; Ren, Y.X.; Tur, M.; Kristensen, P.; Huang, H.; Willner, A.E.; Ramachandran, S. Terabit-Scale Orbital Angular Momentum Mode Division Multiplexing in Fibers. *Science* **2013**, *340*, 1545–1548.
17. Xie, Z.W.; Lei, T.; Li, F.; Qiu, H.D.; Zhang, Z.C.; Wang, H.; Min, C.J.; Du, L.P.; Li, Z.H.; Yuan, X.C. Ultra-broadband on-chip twisted light emitter for optical communications. *Light-Sci. Appl.* **2018**, *7*, 6.

18. Rubinsztein-Dunlop, H.; Forbes, A.; Berry, M.V.; Dennis, M.R.; Andrews, D.L.; Mansuripur, M.; Denz, C.; Alpmann, C.; Banzer, P.; Bauer, T. Roadmap on structured light. *J. Opt.* **2016**, *19*, 013001.
19. Beijersbergen, M.W.; Coerwinkel, R.P.C.; Kristensen, M.; Woerdman, J.P. Helical-wavefront laser beams produced with a spiral phaseplate. *Opt. Commun.* **1994**, *112*, 321–327.
20. Biener, G.; Niv, A.; Kleiner, V.; Hasman, E. Formation of helical beams by use of Pancharatnam-Berry phase optical elements. *Opt. Lett.* **2002**, *27*, 1875–1877.
21. Chen, L.X.; Zhang, Y.Y. Research progress on preparation, manipulation, and remote sensing applications of high-order orbital angular momentum of photons. *Acta Phys. Sin.* **2015**, *64*, 191.
22. Alpmann, C.; Schlickriede, C.; Otte, E.; Denz, C. Dynamic modulation of Poincaré beams. *Sci. Rep.* **2017**, *7*, 9.
23. Ren, Y.; Wang, C.; Liu, T.; Wang, Z.K.; Yin, C.Z.; Qiu, S.; Li, Z.M.; Wu, H. Polygonal shaping and multi-singularity manipulation of optical vortices via high-order cross-phase. *Opt. Express* **2020**, *28*, 26257–26266. [[PubMed](#)]
24. Liu, M.Z.; Huo, P.C.; Zhu, W.Q.; Zhang, C.; Zhang, S.; Song, M.W.; Zhang, S.; Zhou, Q.W.; Chen, L.; Lezec, H.J.; et al. Broadband generation of perfect Poincaré beams via dielectric spin-multiplexed metasurface. *Nat. Commun.* **2021**, *12*, 9.
25. Lubk, A.; Clark, L.; Guzzinati, G.; Verbeeck, J. Topological analysis of paraxially scattered electron vortex beams. *Phys. Rev. A* **2013**, *87*, 8.
26. Zhou, Y.Q.; Yin, Y.; Yuan, Y.D.; Lin, T.G.; Huang, H.H.; Yao, L.S.; Wang, X.Q.; Tam, A.M.W.; Fan, F.; Wen, S.C. Liquid crystal Pancharatnam-Berry phase lens with spatially separated focuses. *Liq. Cryst.* **2019**, *46*, 995–1000.
27. Zheng, C.; Li, J.; Liu, J.; Li, J.; Yue, Z.; Li, H.; Yang, F.; Zhang, Y.; Zhang, Y.; Yao, J. Creating Longitudinally Varying Vector Vortex Beams with an All-Dielectric Metasurface. *Laser Photonics Rev.* **2022**, *16*, 2200236.
28. Xu, C.T.; Chen, P.; Zhang, Y.H.; Fan, X.Y.; Lu, Y.Q.; Hu, W. Tunable band-pass optical vortex processor enabled by wash-out-refill chiral superstructures. *Appl. Phys. Lett.* **2021**, *118*, 151102.
29. Zhang, H.; Duan, W.; Wei, T.; Xu, C.; Hu, W. Broadband Multichannel Optical Vortex Generators via Patterned Double-Layer Reverse-Twist Liquid Crystal Polymer. *Crystals* **2020**, *10*, 882.
30. Xu, C.T.; Liu, B.H.; Peng, C.; Chen, Q.M.; Chen, P.; Sun, P.Z.; Zheng, Z.G.; Lu, Y.Q.; Hu, W. Heliconical Cholesterics Endows Spatial Phase Modulator with an Electrically Customizable Working Band. *Adv. Opt. Mater.* **2022**, *10*, 7.
31. Zheng, C.; Li, J.; Li, J.; Yue, Z.; Wang, S.; Li, M.; Zhao, H.; Hao, X.; Zang, H.; Zhang, Y. All-silicon chiral metasurfaces and wavefront shaping assisted by interference. *Sci. China-Phys. Mech. Astron.* **2021**, *064*, 114212.
32. Feng, W.B.; Ye, M. Positive-Negative Tunable Liquid Crystal Lens of Rectangular Aperture. *IEEE Photonics Technol. Lett.* **2022**, *34*, 795–798.
33. Fuh, A.Y.G.; Ko, S.W.; Huang, S.H.; Chen, Y.Y.; Lin, T.H. Polarization-independent liquid crystal lens based on axially symmetric photoalignment. *Opt. Express* **2011**, *19*, 2294–2300. [[PubMed](#)]
34. Li, L.M.; Zeng, X.Y.; Gu, M.N.; Zhang, Y.Q.; Sun, R.; Zhang, Z.H.; Cui, G.S.; Zhou, Y.X.; Cheng, C.F.; Liu, C.X. Plasmonic Metasurfaces for Superposition of Profile-Tunable Tightly Focused Vector Beams and Generation of the Structured Light. *Photonics* **2023**, *10*, 18.
35. Kovalev, A.A.; Kotlyar, V.V. Orbital Angular Momentum of Superpositions of Optical Vortices Perturbed by a Sector Aperture. *Photonics* **2022**, *9*, 14.
36. Hernandez-Garcia, C.; Vieira, J.; Mendonca, J.T.; Rego, L.; Roman, J.S.; Plaja, L.; Ribic, P.R.; Gauthier, D.; Picon, A. Generation and Applications of Extreme-Ultraviolet Vortices. *Photonics* **2017**, *4*, 17.
37. Gaffoglio, R.; Cagliero, A.; Vecchi, G.; Andriulli, F.P. Vortex Waves and Channel Capacity: Hopes and Reality. *IEEE Access* **2018**, *6*, 19814–19822. [[CrossRef](#)]
38. Roichman, Y.; Sun, B.; Roichman, Y.; Amato-Grill, J.; Grier, D.G. Optical forces arising from phase gradients. *Phys. Rev. Lett.* **2008**, *100*, 4.
39. Li, J.S.; Zhuang, S.L.; Huang, C.Q. Gradient force evolution of Gaussian beam induced by a phase plate. *Opt. Lasers Eng.* **2008**, *46*, 595–600.
40. Shen, Y.J.; Wang, X.J.; Xie, Z.W.; Min, C.J.; Fu, X.; Liu, Q.; Gong, M.L.; Yuan, X.C. Optical vortices 30 years on: OAM manipulation from topological charge to multiple singularities. *Light-Sci. Appl.* **2019**, *8*, 29.
41. Banerji, A.; Singh, R.P.; Banerjee, D.; Bandyopadhyay, A. Entanglement propagation of a quantum optical vortex state. *Opt. Commun.* **2016**, *380*, 492–498. [[CrossRef](#)]
42. Lin, T.G.; Zhou, Y.Q.; Yuan, Y.D.; Fu, W.X.; Yao, L.S.; Huang, H.H.; Fan, F.; Wen, S.C. Transflective spin-orbital angular momentum conversion device by three-dimensional multilayer liquid crystalline materials. *Opt. Express* **2018**, *26*, 29244–29252. [[CrossRef](#)] [[PubMed](#)]
43. Lin, T.G.; Xie, J.; Zhou, Y.J.; Zhou, Y.Q.; Yuan, Y.D.; Fan, F.; Wen, S.C. Recent Advances in Photoalignment Liquid Crystal Polarization Gratings and Their Applications. *Crystals* **2021**, *11*, 22. [[CrossRef](#)]

44. Lou, S.Z.; Zhou, Y.Q.; Yuan, Y.D.; Lin, T.G.; Fan, F.; Wang, X.Q.; Huang, H.H.; Wen, S.C. Generation of arbitrary vector vortex beams on hybrid-order Poincare sphere based on liquid crystal device. *Opt. Express* **2019**, *27*, 8596–8604. [[CrossRef](#)]
45. Ye, X.L.; Zeng, T.B.; Liu, S.; Fan, F.; Wen, S.C. Optical imprinting subwavelength-period liquid crystal polarization gratings with dual-twist templates. *Opt. Lett.* **2023**, *48*, 2078–2081. [[CrossRef](#)]

Disclaimer/Publisher’s Note: The statements, opinions and data contained in all publications are solely those of the individual author(s) and contributor(s) and not of MDPI and/or the editor(s). MDPI and/or the editor(s) disclaim responsibility for any injury to people or property resulting from any ideas, methods, instructions or products referred to in the content.